Energy Conversion and Management 331 (2025) 119655

Contents lists available at ScienceDirect

Energy Conversion and Management

journal homepage: www.elsevier.com/locate/enconman

Research paper

Comparative study of a new semi-empirical model of the proton exchange membrane fuel cell for online prognostics applications

L.M. Perez [a,b,*], Samir Jemei [a], Loïc Boulon [b], Alexandre Ravey [c], Mohsen Kandidayeni [b], Javier Solano [d]

[a] Université de Franche-Comté, UTBM, CNRS, institute FEMTO-ST, FCLAB, Belfort, F-90000, France
[b] Hydrogen Research Institute, Electrical and Computer Engineering Department, Université Du Québec a Trois-Rivières, Québec, G8Z 4M3, Canada
[c] UTBM, CNRS, institute FEMTO-ST, FCLAB, Belfort, F-90000, France
[d] European Institute for Energy Research (EIFER), Emmy-Noether-Str. 11, Karlsruhe, 76131, Germany

ARTICLE INFO

Keywords:
Proton exchange membrane fuel cell
Parameter estimation
Pelican optimization algorithm
Model identification
Prognostic and degradation
Filter algorithm

ABSTRACT

The prognostic of the proton exchange membrane fuel cell is a current topic of research. Consequently, the complexity of its degradation mechanisms has led to the development of semi-empirical models to improve predictive analysis. The accurate estimation of parameters for these models is a challenging task due to their multivariate, nonlinear, and complex characteristics. This work proposes a new semi-empirical model of the proton exchange membrane fuel cell and compares it with a widely used model in the literature. Unlike other similar studies, this comparison not only focuses on minimizing the sum of squared errors in relation to the experimental data but also evaluates the variation in the solution set and the computational effort involved. For both models, the unknown parameters are estimated using the recent Pelican Optimization Algorithm. Four datasets are used to evaluate the development of the proposed model and the selected benchmark model. The first three datasets are open-access and well-recognized in academic literature, whereas the fourth dataset was obtained from a developed experimental test bench. The results show that the proposed model achieves high accuracy, with a mean absolute percentage error lower than 0.89% and the sum of squared errors below 0.9272 for all the studied scenarios. This model reduces parameter variation and decreases the relative standard deviation by over 12.7% compared to the utilized benchmark model for the first three datasets. Hence, the proposed model not only improves the precision of the estimated parameters without a notable increase in error but also reduces the computational load by at least 21.7% across all case studies.

1. Introduction

With the ongoing global climate change and its consequences, researchers are working to advance the development of alternative energy sources that have a lower environmental impact than traditional fossil fuels [1]. The use of hydrogen as an alternative energy source has attracted the interest of various governments and international organizations [2]. Fuel Cells (FCs) are devices that generate electricity, heat, and water by using hydrogen as fuel and oxygen as an oxidant. In recent years, various types of FCs have been developed [3]. Among these, the Proton Exchange Membrane Fuel Cell (PEMFC) stands out as one of the most popular [4]. Its popularity stems from characteristics like high energy density, zero pollutant emissions, a solid proton exchange membrane, low operating temperature, and fast start-up [5].

The characteristics of PEMFCs make them a popular choice for developing Fuel Cell Hybrid Electric Vehicles (FCHEVs) [6]. Moreover, PEMFC systems offer significant advantages when both electrical and thermal energy are required, particularly in cogeneration setups that integrate PEMFCs with an Organic Rankine Cycle (ORC) [7]. These integrated systems improve both efficiency and economic performance [8], largely due to effective thermodynamic management and the recovery of waste heat from components such as the PEMFC stack, air compressor, and electrochemical reaction byproducts [9]. However, the limited lifespan of PEMFCs remains a significant technical challenge for future applications, as highlighted by many researchers [10]. This challenge arises from the dynamic operating conditions and varying load cycles PEMFCs face in these applications [11]. To address this, new Prognostic and Health Management (PHM) techniques are

* Corresponding author at: Hydrogen Research Institute, Electrical and Computer Engineering Department, Université Du Québec a Trois-Rivières, Québec, G8Z 4M3, Canada.
E-mail address: Luis.Miguel.Perez.Archila@uqtr.ca (L.M. Perez).

https://doi.org/10.1016/j.enconman.2025.119655
Received 15 March 2024; Received in revised form 8 February 2025; Accepted 13 February 2025
Available online 27 February 2025

being developed to estimate and forecast the PEMFC's health [12]. These techniques, applied in control, design, and energy management strategies, aim to reduce PEMFC degradation [13].

Nonetheless, PEMFC is a complex device in which multiple reactions occur simultaneously. The physical representation of this device involves a multi-physics model with thermal, electrical, chemical, and fluid mechanical components [14]. Moreover, in real-time applications such as vehicles, PHM techniques are generally limited by computing resources, computation time, and model complexity [15]. Therefore, the PEMFC, being a component of complex systems like FCHEVs, requires a balanced model that considers both simplicity and accuracy [16]. In the literature, regarding the utilized modeling techniques, the studies in PHM techniques are broadly grouped into three main categories: model-based, data-based, and hybrid approaches [17].

Model-based techniques, also known as white box models, provide the most accurate and detailed physical representations of PEMFC behavior through algebraic and differential equations grounded in physical laws [18]. However, the complexity of these models and their high computational demands make them impractical for real-time applications such as control, energy management, and fault detection [19]. Consequently, these models are more appropriate for design and diagnostic purposes [20].

In contrast, data-based techniques, or black box models, leverage learning algorithms to analyze historical operational data, identifying patterns to forecast the future health of the PEMFC [21]. Despite their utility, these methods are highly dependent on large datasets for training. This dependency can prolong the time required to obtain accurate predictions, thus limiting their effectiveness for real-time applications [22]. Additionally, most data-based PHM techniques rely on complex neural networks, demanding significant computational resources [17].

To address the limitations of both approaches, hybrid techniques, which integrate elements from model-based and data-based methods, have been developed [23]. These hybrid techniques employ semi-empirical (gray box) models to simplify system behavior through empirical adjustments. Although they achieve a satisfactory level of accuracy, it remains lower than that of purely physics-based models, as semi-empirical models account only for the primary factors and physical processes [24]. Semi-empirical models consist of a set of algebraic equations based on physical principles, supplemented by empirical constants and parameters that emulate certain physical variables that are technically unmeasurable [25]. By offering a balance between complexity and computational efficiency, hybrid models are particularly suited for real-time applications, where computational resources and time are constrained [26].

The applications of the semi-empirical models and adaptive filter algorithms have recently been applied in the forecast of PEMFC health indicators [27]. A semi-empirical model for identification and aging parameters is applied in an Extended Kalman Filter (EKF) for PEMFC lifespan prognostics [28]. Similarly, Pei et al. [29] introduced a nonlinear empirical model to estimate health indices based on voltage stack changes. Equivalent circuit models calibrated with experimental data are another approach. In [30], such models are employed with Electrochemical Impedance Spectroscopy (EIS) data, while in [31], a static and dynamic EIS-based model is proposed for aging monitoring. In [32] Electrochemical Surface Area (ECSA) is used to predict degradation, and in [33], exponential and logarithmic empirical models are integrated into particle filters for prognostics applications. The model proposed by Amphlett et al. [34] has been extensively utilized in prognostic applications. Ren et al. [35] integrated it into an Unscented Kalman Filter (UKF) for degradation forecasting. Similarly, [36] employed it with a Smooth Variable Structure Filter and Kalman Filter (SVSF-KF), while Guo et al. [37] used it with a Marginalized Particle Filter (MPF) for voltage stack prognostics. These semi-empirical models enhance the balance between accuracy and computational efficiency, supporting real-time PEMFC health monitoring and prognostics. Therefore, this work focuses on semi-empirical models used in hybrid PHM techniques, and a brief review of them will be presented in Table 1.

The data in Table 1 show that the semi-empirical model proposed by Amphlett et al. [34] is widely used in prognostic methods, establishing it as a benchmark model. Additionally, the voltage stack is the most common health indicator for PEMFCs. Nevertheless, other health indices such as empirical model parameters have been proposed to represent degradation in the voltage stack. In the prognostic methods presented in Table 1, semi-empirical models and adaptive filter-based algorithms are utilized to adjust empirical parameters over time and under varying operating conditions. This time-based tracking enables researchers to estimate PEMFC degradation without relying on direct measurements such as the membrane water content, which are often technically unavailable [38].

A key aspect of these prognostic approaches is the identification process, which serves as an essential first step to ensure accurate degradation predictions. It involves the selection of a semi-empirical model and the estimation of the initial parameter values, which provide a reference point for predicting and estimating degradation in the PEMFC [39]. This selection should consider factors such as the intended application, available computational resources, and the effects of degradation phenomena [40]. However, semi-empirical models often fail to capture all the physical processes influencing PEMFC operation and degradation. To address these limitations, identification algorithms are employed to incorporate more complex and neglected phenomena. These algorithms minimize the error between the model and the experimental data, allowing accurate simulations of PEMFC behavior [26].

In identification, a set of parameters is estimated to represent the initial state of health, which is vital for future prediction of degradation [25]. Thus, identifying accurate model parameters is essential, particularly for determining initial values for the prognostic algorithm [41]. Estimating these parameters from polarization curves involves solving a least-squares optimization problem, which is nonlinear, multivariable, and has multiple local minima. This makes traditional deterministic and single-agent optimization methods less effective for parameter estimation [42]. As a result, meta-heuristic optimization algorithms have emerged as a prominent approach for fitting PEMFC models to polarization curves and accurately identifying the parameters of these models. A variety of algorithms have been employed for PEMFC parameter estimation, including meta-heuristic optimization techniques used to fit PEMFC models to polarization curves. Prior research has explored algorithms such as the Enhanced Bald Eagle Search (EBES) [43], Flower Pollination Algorithm (FPA) [44], Tunicate Swarm Algorithm (TSA) [45], Water Cycle Algorithm (WCA) [46], Shark Smell Optimizer (SSO) [47], Grey Wolf Optimizer (GWO) [48], Modified Farmland Fertility Algorithm (MFFA) [49], Bonobo Optimizer (BO) [50], Fractional-Order Modified Harris Hawks Optimizer (FMHHO) [51], Marine Predators Algorithm (MPA) [52], Whale Optimization Algorithm (WOA) [53], Grasshopper Optimization Algorithm (GOA) [54], Circle Search Algorithm (CSA) [55], Bald Eagle Search (BES) [56], Improved Artificial Hummingbird Algorithm (IAHA) [57], Artificial Bee Colony Differential Evolution (ABCDE) [42]. These algorithms, along with their corresponding applications to PEMFC parameter identification, are summarized in Table 2.

The research presented in Table 2 utilizes the Amphlett semi-empirical model to represent PEMFC performance, adjusting the models based on polarization curves. Most studies focus on improving the application of meta-heuristic algorithms and exploring new methods to better characterize these models. However, some studies provide different solution sets for the same experimental data, with varying levels of precision, as is shown in Table 2. These studies tend to overlook the internal structure of the models and the accuracy of the estimated parameters.

Table 1
Resume of semi-empirical models used in prognostic hybrid techniques.

	Year	Model	Fitting algorithm	Health indicator	Operating conditions	Accuracy	Prognostic horizon
[28]	2016	Semi-empirical voltage-current model	Extended Kalman Filter	Voltage stack	Stationary	Percentage error of RUL $\leq 10\%$	1050 h
[29]	2019	First-order control system	A proposed method	Voltage stack	Stationary	Mean Relative Error = 2.53%	800 h
[35]	2020	Semi-empirical model proposed by Amphlett et al.	Unscented Kalman Filter	Voltage stack	Dynamic	Percentage error of RUL $\leq 2\%$	1000 s
[30]	2020	Analytical equivalent circuit model	Nonlinear least square method	Electrochemical Impedance Spectroscopy	Stationary	Scores SOH = 3.941×10^{-6}	333 h
					Dynamic	Scores SOH = 8.202×10^{-6}	350 h
[32]	2021	Semi-empirical voltage-current model with aging parameters	Least square method	Voltage stack + 5 empirical parameters	Dynamic	RMSE = 0.0354	500 h
[31]	2021	Semi-empirical voltage-current model	Trust-Region-Reflective least squares	Voltage stack + 4 empirical parameters	Dynamic	Maximum relative error = 1%	700 h
[33]	2022	Exponential and logarithmic empirical model	Particle filter	Voltage stack + 4 empirical parameters	Dynamic	nRMSE = $1.17\times^{-2}$	350 h
[36]	2022	Semi-empirical model proposed by Amphlett et al.	Smooth variable structure filter and Kalman filter	Voltage stack	Dynamic	MAPE = 0.0169	600 s
[37]	2023	Semi-empirical model proposed by Amphlett et al.	Marginalized particle filter	Voltage stack	Dynamic	MSE = 4.9848×10^{-4}	1000 s

Table 2
Resume of meta-heuristic optimization algorithms applied in PEMFC parameter identification.

Reference	Algorithm	PEMFC power (W)	Parameters for the lowest SSE						
			ξ_1	$\xi_2 \times 10^{-3}$	$\xi_3 \times 10^{-5}$	$\xi_4 \times 10^{-4}$	λ	$R_C \times 10^{-4}$	β
[43]	EBES	BCS-500	−1.1997	3.3559	5.44	−1.9302	20.8772	1.00	0.0161
[44]	FPA	BCS-500	−0.9851	2.8000	4.46	−2.3200	17.4598	1.66	0.0697
[45]	TSA	250	−1.0958	3.0915	5.2525	−1.5565	23	1.16	0.0542
[46]	WCA	250	−1.141	3.8409	8.9942	−1.558	23	1.00	0.0545
[47]	SSO	250	−1.0554	3.7953	9.80	−1.1755	24	1.09	0.0136
[48]	GWO	250	−1.0564	3.7953	9.80	−1.1755	24	1.09	0.0136
[49]	MFFA	250	−1.0018	2.6120	3.9959	−1.5587	23	1.00	0.0546
[50]	BO	250	−1.1997	3.0189	3.60	−1.5587	23	1.00	0.0546
[51]	FMHHO	SR12-500	−0.8532	3	7.8169	−0.9540	23	1.0201	0.15222
[52]	MPA	SR12-500	−1.028359	3.898047	9.80	−0.9540	23	6.7231	0.1753
[53]	WOA	Ballard-5000	−1.1978	4.4183	9.7214	−1.6273	23	1.002	0.0136
[54]	GOA	Ballard-5000	−0.8532	3.4173	9.8	−1.5955	22.8458	1.00	0.0136
[55]	CSA	Ballard-5000	−1.1813	3.5691	3.9929	−1.6283	23	1.00	0.0136
[56]	BES	PS6-6000	−1.1490	3.3487	3.6	−9.54	13.0975	1.00	0.0136
[57]	IAHA	PS6-6000	−0.8541	2.5	3.6	−9.54	13.4654	1.00	0.0136
[42]	ABCDE	PS6-6000	−1.0781	33.8556	5.9698	−0.9540	13.0947	1.00	0.0136

Other works dive deeper into PEMFC models, offering comparisons between various approaches to highlight their strengths and weaknesses [58]. Yet, these studies also fail to explore the variation in the estimated parameters. As a result, research on parameter variation during model identification remains scarce [59]. Additionally, disparities in the computational efficiency of different semi-empirical models have received little attention in the context of PEMFC PHM [23]. For some PHM techniques used in online applications, model complexity is constrained by the need for rapid computations, making computational time a critical factor in algorithm development [22].

In this work, a comparative study is performed between a developed semi-empirical PEMFC model and a well-known benchmark model from the literature, focusing on the accuracy, precision of the estimated parameters, and computational efficiency of both models. This comparison utilizes four datasets, three previously reported in the literature, and one experimental dataset developed for this study. The focus is on assessing the accuracy and precision of the fitting algorithm, as well as the variation in the estimated parameters. The Pelican Optimization Algorithm (POA), a novel meta-heuristic algorithm for PEMFC parameter identification, is used to fit the models to the datasets effectively. The algorithm is iterated multiple times to calculate the mean and standard deviation of both the objective function and the estimated parameters.

The remainder of this article is structured as follows: Section 2 introduces the two models being compared, the optimization method used, and experimental data. Simulation results for both models are presented in Section 3. Finally, conclusions are given in Section 4.

2. Materials and methods

Modeling of the PEMFC is often used to estimate its performance and state of health [60]. For this estimation, an inverse problem is solved to calibrate the model using the polarization test [61]. In the

polarization test, all operating conditions of the FC, such as temperature and pressure at the electrodes, are kept constant, except for the stack current. The stack current is adjusted to different levels, varying within the range from 0 A to the nominal current. The stack voltage output is measured for each set value of the current, generating an experimental graph (voltage vs. current) known as the polarization curve [58].

In this article, two models are compared: a reference model commonly used in the literature and a proposed model aimed at improving precision, accuracy, and computational complexity. Both models are calibrated against the polarization curve to determine the model parameters. An estimation of the initial state of health of the PEMFC is provided by this initial set of parameters, along with the model. This initial estimation is considered a preliminary stage of the prognostic algorithms, known as the identification process.

The materials and methods used in this article are described as follows: the benchmark model subsection introduces the model commonly employed in the literature to estimate the initial state of health of PEMFCs in prognostic techniques. The proposed model subsection presents the model designed for comparison with the benchmark model and to perform parameter estimation by fitting both models to the polarization curve. The next subsection details the formulation used to fit the models to the polarization curve, estimating the initial state of health through the initial parameter values. The optimization algorithm subsection describes the algorithm employed to solve the optimization problem. Finally, the experimental setup subsection details the setup used to obtain the polarization curve, which is critical for fitting the models and evaluating the accuracy and precision of the estimated parameters.

2.1. Benchmark model

Several studies have investigated the use of meta-heuristic algorithms for estimating the parameters of the FC semi-empirical model proposed by Amphlett et al. [34]. This model simulates the electrochemical behavior of a fuel cell as a subtraction of the reversible voltage (E_{Nernst}) from three distinct loss factors: activation losses (V_{act}), ohmic losses (V_{ohm}), and concentration losses (V_{con}) [62]. Each of these factors predominantly influences a specific region of the I-V polarization curve. Activation losses primarily affect the low current region (values close to zero), ohmic losses significantly impact the middle region, and concentration losses contribute most to the high current region (values near the maximum current I_{max}). This model is scalable, meaning that the model of a single cell can be multiplied by the number of cells (N_{cells}) to obtain the stack model as shown in Eq. (1).

$$V_{stack} = N_{cells} \cdot (E_{Nernst} - V_{act} - V_{ohm} - V_{con}) \tag{1}$$

The reversible voltage is given in Eq. (2), so it depends on the temperature of the PEMFC (T) and the partial pressures of the hydrogen and oxygen, respectively (P_{H_2}, P_{O_2}).

$$E_{Nernst} = 1.229 - 0.85 \times 10^{-3} \cdot (T - 298.15) + 4.3085 \times 10^{-5} \cdot T \cdot \left[ln(P_{H2}) + \frac{1}{2} ln(P_{O2})\right] \tag{2}$$

The partial pressures of the reactants are obtained from Eq. (3), Eq. (4), and Eq. (5), where, $P^{sat}_{H_2O}$ is the saturation pressure of the water vapor; RH_c and RH_a are the relative humidity of steam at the cathode and anode, respectively; P_a and P_c are the channel pressure (atm) at the anode and cathode, respectively; I_{fc} is the output current from the fuel cell stack; and A is the active surface area of the membrane.

$$log_{10}\left(P^{sat}_{H_2O}\right) = 2.95 \times 10^{-2} \cdot (T - 273.15) - 9.18 \times 10^{-5} \cdot (T - 273.15)^2 + 1.44 \times 10^{-7} \cdot (T - 273.15)^3 - 2.18 \tag{3}$$

$$P_{O_2} = \frac{P_c - (RH_c \cdot P^{sat}_{H_2O})}{1 + \frac{0.79}{0.21} \cdot exp\left(\frac{0.291 \cdot (I_{fc}/A)}{T^{0.832}}\right)} \tag{4}$$

$$P_{H_2} = 0.5 \cdot (RH_a \cdot P^{sat}_{H_2O}) \cdot \left[\frac{1}{exp\left(\frac{1.635 \cdot (I_{fc}/A)}{T^{1.334}}\right) \cdot \frac{RH_a \times P^{sat}_{H_2O}}{P_a}} - 1\right] \tag{5}$$

The activation voltage drop (V_{act}) is specified in Eq. (6), and the variables $\xi_1, \xi_2, \xi_3, \xi_4$ are semi-empirical coefficients; C_{O_2} is the concentration of oxygen at the surface of the cathode ($mol \cdot cm^{-3}$) defined in Eq. (7).

$$V_{act} = -[\xi_1 + \xi_2 \cdot T + \xi_3 \cdot T \cdot ln\left(C_{O_2}\right) + \xi_4 \cdot T \cdot ln\left(I_{fc}\right)] \tag{6}$$

$$C_{O_2} = \frac{P_{O_2}}{5.08 \cdot 10^6 \cdot exp\left(\frac{-498}{T}\right)} \tag{7}$$

The second loss factor is the ohmic loss (V_{ohm}) which is calculated based on Ohm's law and is described in Eq. (8), Eq. (9), and Eq. (10).

$$V_{ohm} = I_{fc} \cdot (R_M + R_C) \tag{8}$$

$$R_M = \frac{\rho_M \cdot l}{A} \tag{9}$$

$$\rho_M = \frac{181.6 \cdot \left[1 + 0.03 \cdot \frac{I_{fc}}{A} + 0.062 \cdot \left(\frac{T}{303}\right)^2 \cdot \left(\frac{I_{fc}}{A}\right)^{2.5}\right]}{\left[\lambda - 0.634 - 3\left(\frac{I_{fc}}{A}\right)\right] \cdot exp\left(4.18 \cdot \left(\frac{T-303}{T}\right)\right)} \tag{10}$$

In the equations above, R_M and R_C are membrane and contact resistance, respectively (Ω). l symbolizes the effective thickness of the membrane (cm), ρ_M is the resistivity of the membrane (Ω cm), λ is an adjustable parameter that models the water content of the membrane and has a range between 13 and 24. Finally, the concentration losses are described in Eq. (11), where β is the adjusting parametric coefficient, J is the current density, and J_{max} is the maximum current density (A/cm^2).

$$V_{con} = -\beta \cdot ln\left(1 - \frac{J}{J_{max}}\right) \tag{11}$$

2.2. Proposed model

The model proposed in this work defines the stack voltage (V_{stack}) and the reversible voltage (E_{Nernst}) using the same equations as the benchmark model. Nevertheless, the three polarization loss factors, namely activation losses, ohmic losses, and concentration losses, are redefined to incorporate certain approximations and simplifications. For activation losses, these are the primary contributors to the voltage drop observed in low-current regions during polarization tests. Such losses arise from the energy required to overcome the activation barriers that initiate oxidation and reduction reactions at the electrodes. Additionally, at open-circuit voltage, further losses occur due to hydrogen fuel diffusion from the anode to the cathode through the membrane without the anodic reaction. Although proton exchange membranes are largely impermeable to hydrogen, this diffusion still contributes to voltage loss [63]. The effects of these processes are modeled using Tafel's equation:

$$V_{act} = \frac{RT}{2\alpha F} \cdot ln\left(\frac{I_{fc} + I_{loss}}{I_0}\right) \tag{12}$$

In Eq. (12), I_0 represents the exchange current required to start electrochemical reactions, while I_{loss} denotes the internal leakage current of hydrogen. The parameter α, referred to as the charge transfer coefficient, is determined by the material properties, microstructure, and reaction mechanisms of the electrodes. Constants R and F correspond to the universal gas constant and Faraday's constant, respectively.

Parameters I_0, I_{loss}, and α are difficult to obtain analytically; therefore, they are derived from polarization tests to adapt the activation loss model to the specific characteristics of each PEMFC. Unlike the benchmark model, the parameters ξ_1, ξ_2, and ξ_3 are excluded from this model due to their significant variability, as detailed in Section 3.

Ohmic losses result from resistances to ionic and electronic flow within various components of the stack such as the membrane, gas diffusion layers, current collectors, and interfacial contacts. Among these, the ionic resistance of the membrane is the most significant, while the electronic resistance is comparatively negligible. Ohmic losses result from conduction phenomena within the PEMFC and are commonly modeled using Ohm's law. However, it is challenging to estimate or separate the membrane and contact resistances in practice. In the proposed model, these resistances are combined into an equivalent resistance parameter, R_{eq}, which accounts for the losses associated with ion and electron transport. These losses are expressed as a proportional function of the current:

$$V_{ohm} = I_{fc} \cdot R_{eq} \tag{13}$$

Lastly, concentration losses dominate the high current region of the polarization curve, where reactant depletion near the electrode surfaces inhibits reaction kinetics. This phenomenon typically occurs due to water accumulation in the cathode, the buildup of inert gases such as nitrogen, and the slower diffusion rate of oxygen compared to hydrogen. The proposed model employs the same equation as the benchmark model to represent concentration losses:

$$V_{con} = -\beta_{eq} \cdot ln\left(1 - \frac{I_{fc}}{I_{max}}\right) \tag{14}$$

In Eq. (14), β_{eq} serves as an adjustment parameter comparable to β in the benchmark model. Nevertheless, β_{eq} is defined with an extended range to enhance the accuracy of the model fit. The proposed model redefines the factors contributing to losses and reduces the number of parameters to be estimated from seven to five, compared to the benchmark model. This approach aims to avoid combining unknown parameters within the same loss factor and to lessen the computational burden. Besides, it avoids the need for often unavailable manufacturer data, like membrane thickness and area, especially for certain commercial PEMFCs. However, these approximations also remove certain variables, such as λ, which represent the membrane's water content and carries considerable physical importance.

2.3. Optimization problem

The optimization problem formulated to fit both the benchmark, and the proposed model is a typical least squares problem. The goal of the fitting process is to minimize the Sum of the Squared Errors (SSE) between the experimental voltage (V^{exp}) obtained from the polarization curves and the stack output voltage calculated using the models (V_{stack}).

The V_{stack} depends on the stack output current and the parameters of the model θ. For the benchmark model, the set of unknown parameters is composed of 7 unknown parameters ($\theta = [\xi_1, \xi_2, \xi_3, \xi_4, \lambda, \beta, R_C]$). In the proposed model, the vector of unknown parameters has 5 components ($\theta = [\alpha, I_0, R_{eq}, \beta_{eq}, I_{loss}]$).

The boundaries of the search region to each model are limited to a set of inequalities. For the ith point of a given experimental polarization curve (V_i^{exp}, I_i^{exp}) the objective function is expressed by Eq. (15).

$$\begin{aligned} \min_{\theta} \quad & F_{obj} = \sum_{i=1}^{N} \left(V_i^{exp} - V_{stack}(I_i^{exp}, \theta)\right)^2 \\ \text{Subject to} \quad & \theta_j^{min} \le \theta_j \le \theta_j^{max} \quad \forall j = 1, 2, \ldots, M \end{aligned} \tag{15}$$

In the previous equation, N is the number of points of the polarization curve, M is the number of parameters in the model, j is the index for each component of the set of parameters, θ_j^{min} and θ_j^{max} are the lower and upper limits of the unknown parameters.

Table 3
Boundaries of the search region for the benchmark and proposed model.

Parameters	Lower bound (θ_j^{min})	Upper bound (θ_j^{max})
Benchmark model		
ξ_1	−1.1997	−0.8532
ξ_2	1×10^{-3}	5×10^{-3}
ξ_3	3.6×10^{-5}	9.8×10^{-5}
ξ_4	-2.60×10^{-4}	-9.54×10^{-5}
λ	10	24
β	0.0136	0.5
R_C	1×10^{-4}	8×10^{-4}
Proposed model		
α	0.1	0.9
I_0	1×10^{-8}	10
R_{eq}	1×10^{-4}	100
β_{eq}	1×10^{-5}	0.5
I_{loss}	1×10^{-3}	10

2.4. Optimization algorithm

A minimization problem, as described in Eq. (15), has been formulated to fit the parameters of the PEMFC model to a polarization test. However, this problem requires the application of a global multi-agent optimization algorithm due to the presence of multiple local minima within the solution region. One objective of this research is to evaluate the recent POA and its effectiveness in solving the problem described in Eq. (15). The suggested POA algorithm imitates how pelicans hunt to update potential solutions in two phases: exploration and exploitation. Within the phase of exploration, pelicans recognize and advance toward the prey's position, thereby amplifying the algorithm's capability to examine and explore the search domain. The location of the prey is generated at random, which enhances the overall exploration experience. In the exploitation phase, pelicans spread their wings to catch prey, which improves local search and allows the algorithm to converge on better solutions. In a mathematical context, this refers to the process of refining the solution by examining points that are close to the pelican's position. This nature-inspired meta-heuristic optimization algorithm is deeply described in [64]. POA is an algorithm that has shown promising results in multivariable optimization problems [65–67]. POA presents a lower minimum value and standard deviation of SSE, compared to other algorithms proposed in the literature, as is shown in the next section of results.

In this study, the POA has been configured with a population size (N_{pop}) of 400 particles and two stopping criteria. The first stopping criterion is reaching a maximum number of iterations (M_{ite}) set at 1×10^5. The second criterion ends the iteration cycle when a change in the best objective function value is less than 1×10^{-19} over the last 4×10^3 iterations. These stopping criteria and the population size were selected using a grid search to improve the accuracy of the SSE and its impact on the set of estimated parameters. Concerning the computational complexity of the algorithm is given in [64], and is presented in Eq. (16).

$$O\left(N_{pop} + M_{ite} \cdot (1 + M) \cdot (1 + 2 \cdot N_{pop})\right) \tag{16}$$

In Eq. (16), M represents the number of variables in the optimization problem, which, in this case, corresponds to the number of parameters to be estimated in the model. All the simulations in this work have been conducted on a computer equipped with an i5-10505 CPU and 32 GB of RAM. For the limits for the optimization problem, the solution region is defined by the boundaries provided in Table 3 for both the benchmark and proposed models.

For the benchmark model, the boundaries are defined as in [52]. In the proposed model, the boundaries are defined in this work, taking reference values shown in [63]. To evaluate the two models described in this section, the optimization algorithm will be applied to four datasets

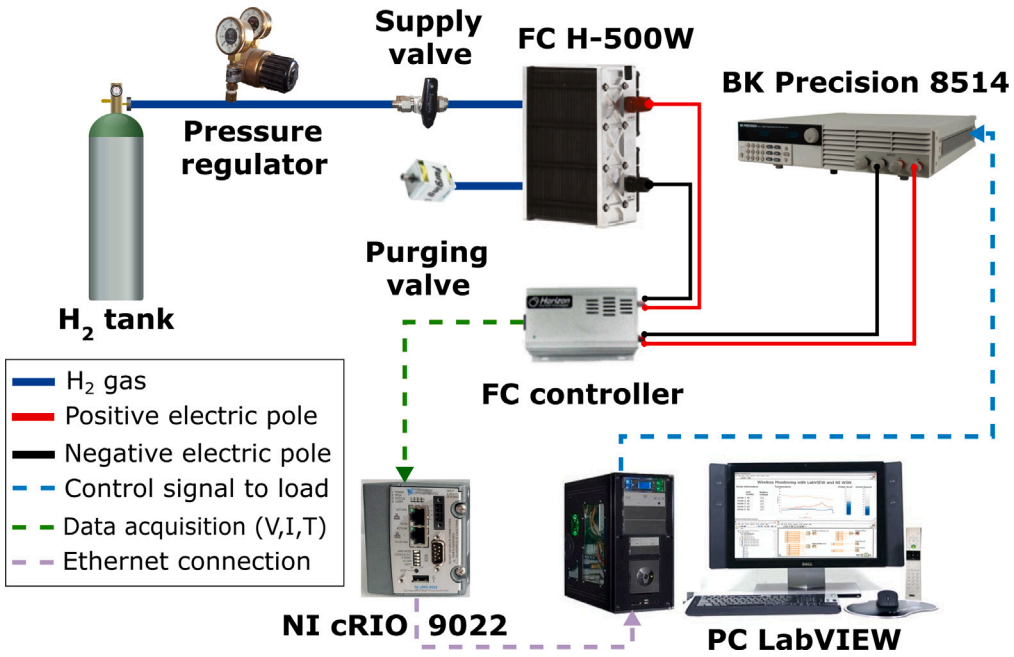

Fig. 1. Experimental setup for the PEMFC Horizon 500 W.

Table 4
Parameters of the commercial PEMFC stacks.

FC stack parameter	BCS-500 W	250 W	SR-12 modular	H-500 W
N_{cells}	32	24	48	36
A (cm^2)	64	27	62.5	52
l (μm)	178	127	25	25
I_{max} (A)	30.016	23.22	42	27
J_{max} (A/cm^2)	0.469	0.860	0.672	0.519
P_{H_2} (atm)	1	1	1.476	0.55
P_{O_2} (atm)	0.2095	1	0.2095	1
T (K)	333	343	323	Variable
RH_a	1.0	1.0	1.0	1.0
RH_c	1.0	1.0	1.0	1.0

to examine the variation and accuracy of the SSE and the estimated parameters. Details about the polarization test and the datasheet of the four case studies are presented in Table 4 [52].

Three of these datasets are well-known, open-access benchmarks frequently used in the literature for estimating PEMFC model parameters. The fourth dataset is derived from a novel experimental setup developed specifically for this study, introduced in the following subsection.

2.5. Experimental set-up

The development of an experimental setup was done to measure the polarization curve of a Horizon open-cathode PEMFC, which has a nominal power of 500 W. Fig. 1 illustrates the complete experimental test bench.

The anode electrode has an inlet valve that supplies the reactant channels with dry hydrogen. To purge accumulated water and nitrogen and replace them with fresh hydrogen, the outlet of the anode is equipped with a valve. Every 10 s, the purge takes place and lasts for 10 ms each time. In the open cathode PEMFC, a forced convection air supply circuit is employed, with the outlet exposed to the environment. In the H-500 W PEMFC stack, air is supplied to the cathode's reactant channel using two axial fans, while heat is removed through forced convection. Controlling the duty cycle of the fans is crucial for managing the airflow rate, which depends highly on the power and temperature of the stack. This open cathode design integrates the air supply, cooling system, and humidification system, thereby reducing the system's complexity, weight, and cost. However, it faces greater challenges in heat and water management compared to closed cathode FCs that utilize water cooling. This mainly stems from the air's limited efficiency in dissipating heat [68]. Consequently, the temperature is variable in this study, unlike other datasets described in the literature.

Hydrogen and air flow in PEMFC are regulated by the integrated controller, which controls the supply valve, purging valve, and cathode fans. According to the generated power of the PEMFC, the hydrogen flow rate ranges from 0 to 11.67×10^{-2} L/s. This PEMFC controller manages the transfer of electrical power from the PEMFC to a programmable load produced by BK Precision, which has a power capacity of 1200 W. Moreover, the controller is connected to an embedded computer NI CompactRIO 9022, which handles the acquisition of the dataset, comprising voltage, current, and temperature. The acquisition system transfers the dataset to a computer with LabVIEW software through an ethernet connection with a frequency of 100 ms.

The measured data corresponds to a polarization curve, which is a relationship between voltage and current. However, in this case, each current value is linked to a specific temperature value, as shown in Fig. 2. Thus, the polarization curve in this case differs from the other scenarios analyzed in this study, where the temperature remains constant all over the polarization test. Gradually increasing the load allows for observation and recording of the voltage and temperature response in the FC. After each increase in the current level, a period of 15 to 25 min is given to the PEMFC to reach a state of equilibrium. It is worth mentioning that the PEMFC's maximum current and nominal power have declined over time due to degradation. The specific values for the nominal current and nominal power are 27 A and 430 W, respectively.

3. Results and discussion

To examine and validate the proposed modeling and optimization algorithm, simulations are run by using four case studies, each with one polarization curve. Statistical analysis has been calculated for each experimental dataset to study the accuracy and precision not only on the fitting error but also on the estimated set of parameters. For each polarization curve, the optimization algorithm was executed 30 times

Table 5
Comparison of the best solution reported in the literature for the BCS-500 W PEMFC stack.

	POA	CSA [55]	ABCDE [42]	FMHHO [51]	MPA [52]	BO [50]
ξ_1	**−1.1997**	−1.1766	−1.1706	−0.8788	−0.9864	−0.9963
ξ_2	$\mathbf{3.22 \times 10^{-3}}$	3.50×10^{-3}	4.09×10^{-3}	3.02×10^{-3}	2.61×10^{-3}	3.40×10^{-3}
ξ_3	$\mathbf{3.60 \times 10^{-5}}$	9.74×10^{-5}	9.75×10^{-5}	8.23×10^{-5}	3.60×10^{-5}	9.77×10^{-5}
ξ_4	$\mathbf{-1.93 \times 10^{-4}}$	-1.93×10^{-4}	-1.93×10^{-4}	-1.91×10^{-4}	-1.93×10^{-4}	-1.93×10^{-4}
λ	**20.8146**	21.3242	20.8772	22.7090	20.8167	20.8185
β	$\mathbf{1.61 \times 10^{-2}}$	1.61×10^{-2}	1.61×10^{-2}	1.53×10^{-2}	1.61×10^{-2}	1.61×10^{-2}
R_C	$\mathbf{1.00 \times 10^{-4}}$	1.46×10^{-4}	1.00×10^{-4}	4.05×10^{-4}	1.00×10^{-4}	1.00×10^{-4}
Comparative statistical results of SSE.						
Best	$\mathbf{1.1556 \times 10^{-2}}$	1.1736×10^{-2}	1.1698×10^{-2}	1.1770×10^{-2}	1.1600×10^{-2}	1.1556×10^{-2}
Worst	$\mathbf{1.1556 \times 10^{-2}}$	–	1.1698×10^{-2}	3.7371×10^{-1}	1.1600×10^{-2}	7.0998
Average	$\mathbf{1.1556 \times 10^{-2}}$	1.2154×10^{-2}	1.1698×10^{-2}	1.3498×10^{-1}	1.1600×10^{-2}	4.8898×10^{-1}
Std. dev.	$\mathbf{5.6860 \times 10^{-17}}$	2.3455×10^{-4}	1.6650×10^{-16}	1.3008×10^{-1}	6.2747×10^{-15}	158.0482

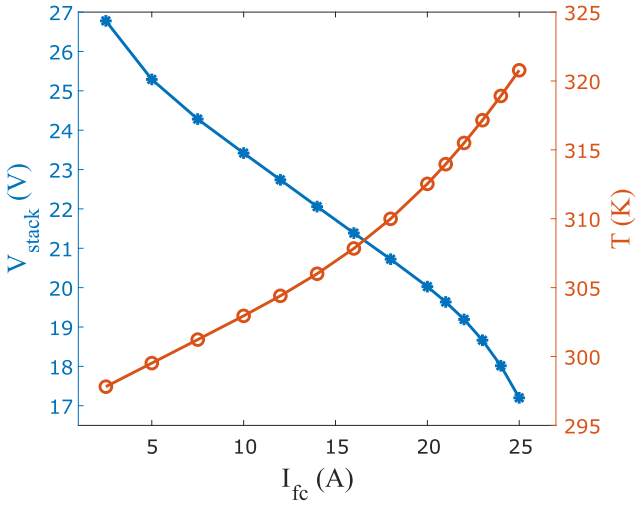

Fig. 2. Experimental data for the H-500 W PEMFC stack in the fourth case of study.

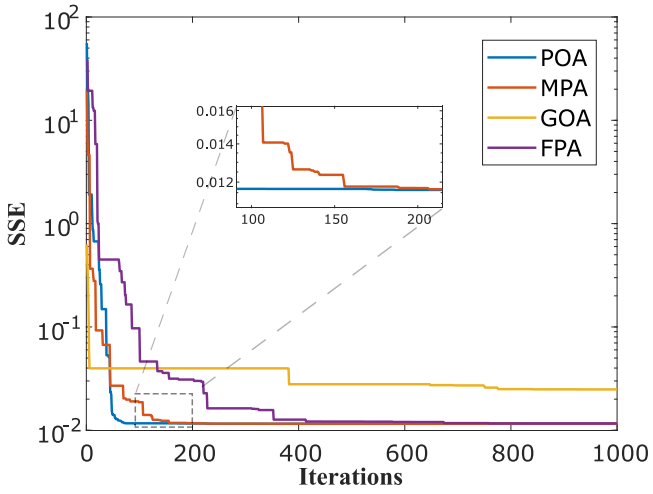

Fig. 3. Convergence of meta-heuristic algorithms for the BCS-500 W PEMFC stack.

to fit each model to the experimental data, estimate the parameters, and determine the fitting error (SSE). These multiple executions of POA are realized to explore the variation of the sets of parameters found by the optimization algorithm. These variations may occur if there are multiple sets of parameters in the solution region of the models that generate the same quasi-optimal value in the objective function. The statistical results are presented in this section.

3.1. The first case study

The dataset for the BCS-500 W PEMFC stack has been used in numerous studies to evaluate the accuracy of various optimization algorithms [42,46,51,52,55]. Therefore, this dataset was selected to compare the performance of the benchmark model, optimized using the POA, with the results reported in previous research. The comparison outcomes are summarized in Table 5.

In Table 5, it is observed that the proposed algorithm finds an equal or lower value for the objective function (SSE). Likewise, the POA achieves the lowest variation of the objective function with a standard deviation of 5.6860×10^{-17}. This low standard deviation, compared to other algorithms, highlights the reliability of the POA, even with a randomly initialized population and consistent SSE results across 30 executions. To explore further dynamic properties, the convergence behavior of the POA is compared with other meta-heuristic algorithms implemented on the same Matlab simulation platform and computing machine. These include the MPA [69], GOA [70], and FPA [71], with results illustrated in Fig. 3.

The POA algorithm has a slower start because, in phase 1, it prioritizes scanning the search space to explore various regions. As a result, GOA and MPA show a faster decrease in the objective function during the first 50 iterations. However, by iteration 150, the POA outperforms the other algorithms, achieving a lower SSE value. This is due to the algorithm's ability to balance exploration and exploitation simultaneously. Therefore, it can be concluded that the POA demonstrates competitive convergence speed compared to other meta-heuristic algorithms. In summary, the POA demonstrates both accuracy and precision in minimizing the fitting error (SSE) when compared to other optimization algorithms in the literature. This optimization algorithm is applied to solve the models and analyze the statistical results with 30 executions. For both models, the settings of the optimization algorithm are the same. The best solutions for the benchmark and the proposed model are illustrated in Fig. 4.

The absolute errors presented in Fig. 4 do not exceed 0.12 V for the two models compared to the maximum voltage of 29 V. The largest absolute error occurs in the middle region, around a current value of 15.73 A, with an approximate percentage error of 0.5% for both models. The Mean Absolute Percentage Error (MAPE) for the benchmark model is 0.06%. Similarly, the MAPE for the simplified model is 0.07%. However, the focus of this paper is not solely on evaluating the accuracy of the objective function. It also includes examining the set of parameters identified by the optimization algorithm and analyzing their variations. A summary of the statistics for the parameter estimates is presented in Table 6. For each parameter of both models, the average (μ), the standard deviation (σ), and the relative standard deviation ($\gamma = |\mu/\sigma|$) are shown.

In Table 6, for the benchmark model, the first three parameters (ξ_1, ξ_2, ξ_3) exhibit a standard deviation that corresponds to 13.5%,

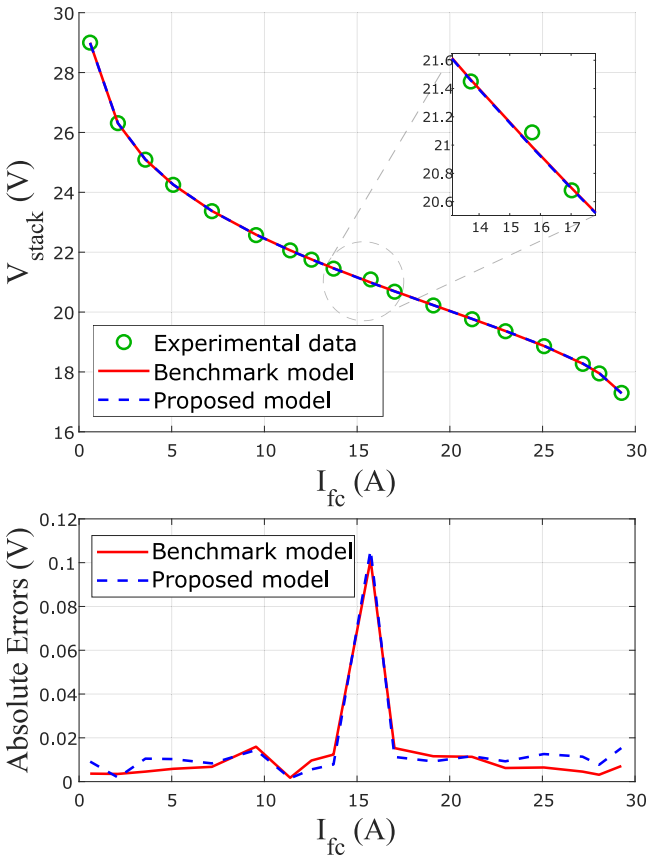

Fig. 4. Best solution for BCS-500 W PEMFC stack obtained from the two analyzed models.

Table 6
Parameters estimated for BCS-500 W PEMFC stack.

Parameter estimated	Mean	Standard deviation	Relative standard deviation
Benchmark model			
ξ_1	-1.0426	1.40×10^{-1}	1.35×10^{-1}
ξ_2	3.29×10^{-3}	5.21×10^{-4}	1.59×10^{-1}
$\boldsymbol{\xi_3}$	$\mathbf{7.08 \times 10^{-5}}$	$\mathbf{2.50 \times 10^{-5}}$	$\mathbf{3.53 \times 10^{-1}}$
ξ_4	-1.93×10^{-4}	1.91×10^{-13}	9.92×10^{-10}
λ	20.8146	1.30×10^{-7}	6.24×10^{-9}
β	1.61×10^{-2}	7.65×10^{-11}	4.75×10^{-9}
R_C	1.00×10^{-4}	2.36×10^{-17}	2.36×10^{-13}
Proposed model			
α	0.2248	2.57×10^{-10}	1.14×10^{-9}
I_0	7.41×10^{-3}	4.46×10^{-11}	6.02×10^{-9}
$\mathbf{R_{eq}}$	$\mathbf{1.96 \times 10^{-3}}$	$\mathbf{1.50 \times 10^{-11}}$	$\mathbf{7.65 \times 10^{-9}}$
β_{eq}	1.68×10^{-2}	8.56×10^{-11}	5.08×10^{-9}
I_{loss}	1.00×10^{-3}	4.58×10^{-16}	4.58×10^{-13}

15.9%, and 35.3% of their respective means. The other parameters for the benchmark model show a standard deviation that is at least nine orders of magnitude lower than the mean. In the proposed model, all parameters show a standard deviation that is nine orders of magnitude lower compared to the mean. In brief, a larger variation is observed in the benchmark model.

To examine how this variation might negatively affect the accuracy of the model's fitting process, a local sensitivity analysis has been conducted on the SSE and is presented in Table 7. In this table, the base case is derived from the best solution presented in Table 5.

From Table 7, the largest variation is seen in the two first parameters (ξ_1, ξ_2) with a relative error of 5.7391×10^3, and 4.5879×10^3 respectively. This suggests that the variation in these parameters could influence the fitting error. The above observations indicate that this low precision in the estimated parameters could be a disadvantage of the benchmark model compared to the proposed model.

Another disadvantage of the benchmark model compared to the proposed one is computing time, averaging 79.58 s for the benchmark model and 41.41 s for the proposed model.

Table 7
Local sensitivity analysis at the optimal point for BCS-500 W PEMFC stack.

Para-meter	% of change	SSE	Relative error (Y)
None	Base case	1.1556×10^{-2}	–
ξ_1	+5	$\mathbf{66.3336}$	$\mathbf{5.7391 \times 10^3}$
	−5	$\mathbf{66.3336}$	$\mathbf{5.7391 \times 10^3}$
ξ_2	+5	53.0303	4.5879×10^3
	−5	53.0303	4.5879×10^3
ξ_3	+5	1.6110	1.3841×10^2
	−5	1.6110	1.3841×10^2
ξ_4	+5	1.2845	1.1016×10^2
	−5	1.2845	1.1016×10^2
λ	+5	6.3423×10^{-2}	4.4883
	−5	7.6085×10^{-2}	5.5839
β	+5	3.6070×10^{-2}	2.1213
	−5	3.6070×10^{-2}	2.1213
R_C	+5	1.1703×10^{-2}	1.2669×10^{-2}
	−5	1.1694×10^{-2}	1.1934×10^{-2}

Table 8
Results for the PEMFC 250 W stack.

Benchmark model		Proposed model	
Best solution			
ξ_1	−0.8817	α	0.2188
ξ_2	2.94×10^{-3}	I_0	8.46×10^{-3}
ξ_3	9.58×10^{-5}	R_{eq}	1.00×10^{-4}
ξ_4	-1.57×10^{-4}	β_{eq}	6.31×10^{-2}
λ	24	I_{loss}	1.22×10^{-1}
β	5.51×10^{-2}		
R_C	1.00×10^{-4}		
Comparative statistical results of SSE.			
Best	6.2465×10^{-1}		$\mathbf{4.9908 \times 10^{-1}}$
Worst	6.2465×10^{-1}		$\mathbf{4.9908 \times 10^{-1}}$
Average	6.2465×10^{-1}		$\mathbf{4.9908 \times 10^{-1}}$
Std. dev.	$\mathbf{5.0626 \times 10^{-16}}$		1.0403×10^{-15}

3.2. The second case study

In the second case study, a PEMFC stack with a nominal power of 250 W has been employed. The description of the data for this FC stack can be found in [51,52]. The POA has been used for solving the two models discussed, and the statistical results for the objective function are presented in Table 8.

In Table 8, the results demonstrate the capability of the POA to achieve accurate solutions for the optimization problem. The SSE values for the proposed model and the benchmark model are 6.25×10^{-1} and 4.99×10^{-1}, respectively. The proposed model achieves an MAPE of 0.89%, while the benchmark model achieves an MAPE of 1.04%. Additionally, Fig. 5 shows the errors for the best solutions of both models, indicating closely matched results with an absolute error below 0.5 V. In the benchmark model, the maximum absolute error is observed at a current level of 3.98 A in the low current region, resulting in an absolute percentage error of 2.1%. For the proposed model, the maximum error occurs at 22 A, with an absolute percentage error of 2.5%. Overall, in this case study, both models demonstrate less accuracy in the activation and concentration regions compared to the ohmic region.

The standard deviation of the minimum value is 14 orders of magnitude smaller than the mean for both models. With this low variation,

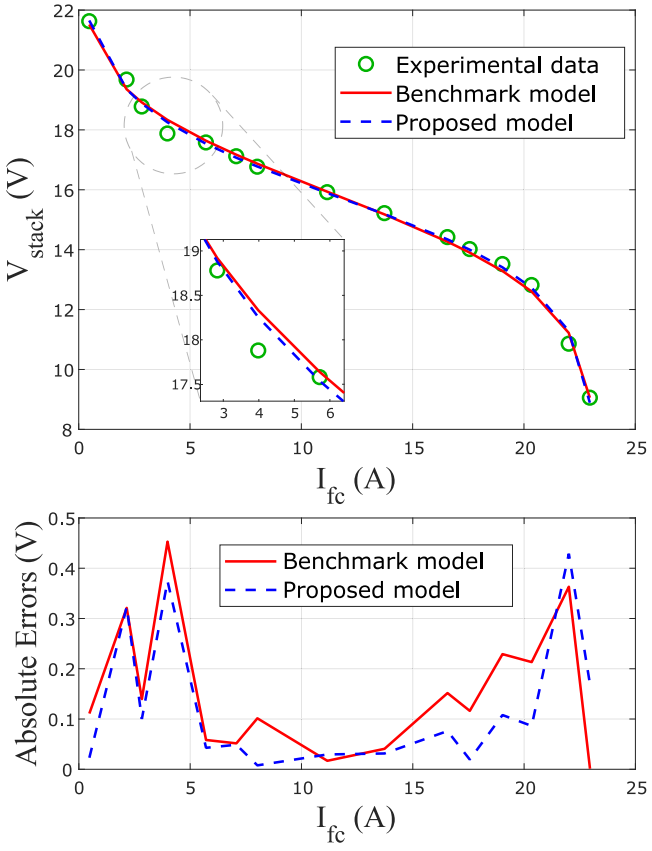

Fig. 5. Best solution for PEMFC 250 W stack obtained from the two analyzed models.

the influence of the variation in the minimized objective function (SSE) under the estimated parameters is negligible. Furthermore, the average computing time for the proposed model is 35.03 s and for the benchmark model is 44.44 s. In short, the proposed model achieves 21.1% less computing time.

Similar to the first case study, the mean and the variation of the optimal set of parameters are evaluated in Table 9. The Relative Standard Deviations (RSD) for the three first parameters of the benchmark model are 12.7%, 14%, and 36%, respectively. For the proposed model, the RSD does not exceed the 7.73×10^{-8}. Therefore, the proposed model presents the lowest variation between the two models.

3.3. The third case study

The third case study focuses on the SR-12 PEMFC stack, which has a nominal power of 500 W, with its data detailed in [42,52]. The best solution obtained by the POA is illustrated in Fig. 6. The absolute error does not exceed 0.66 V in all the voltage range of the polarization curve, which is from 21.4 V to 43.2 V. The MAPE for the proposed and benchmark models is 0.54%, and 0.60%, respectively. Regarding the accuracy of the objective function, the statistics for 30 iterations are presented in Table 10.

Similar to the previous case, the results for the SR-12 500 W PEMFC stack show comparable values for both the minimum and variation of the SSE. There is a difference of −12.23% in the SSE between the proposed model and the benchmark model. In addition, the standard deviation is 14 orders of magnitude smaller than the mean for both models. Similarly, as in the two previous case studies, the proposed model exhibits a lower average computing time, 37.85 s compared to

Table 9
Parameters estimated for the PEMFC 250 W stack.

Parameter estimated	Mean	Standard deviation	Absolute relative standard deviation
Benchmark model			
ξ_1	−1.0099	1.29×10^{-1}	1.27×10^{-1}
ξ_2	2.87×10^{-3}	4.24×10^{-4}	1.48×10^{-1}
ξ_3	$\mathbf{6.37 \times 10^{-5}}$	$\mathbf{2.29 \times 10^{-5}}$	$\mathbf{3.60 \times 10^{-1}}$
ξ_4	-1.57×10^{-4}	4.13×10^{-13}	-2.63×10^{-9}
λ	24	4.15×10^{-14}	1.73×10^{-15}
β	5.51×10^{-2}	1.03×10^{-10}	1.87×10^{-9}
R_C	1.00×10^{-4}	4.60×10^{-18}	4.60×10^{-14}
Proposed model			
α	0.2188	1.09×10^{-9}	5.00×10^{-9}
I_0	8.46×10^{-3}	2.91×10^{-10}	3.45×10^{-8}
R_{eq}	1.00×10^{-4}	8.53×10^{-17}	8.53×10^{-13}
β_{eq}	6.31×10^{-2}	1.46×10^{-10}	2.32×10^{-9}
$\mathbf{I_{loss}}$	**0.1217**	$\mathbf{9.40 \times 10^{-9}}$	$\mathbf{7.73 \times 10^{-8}}$

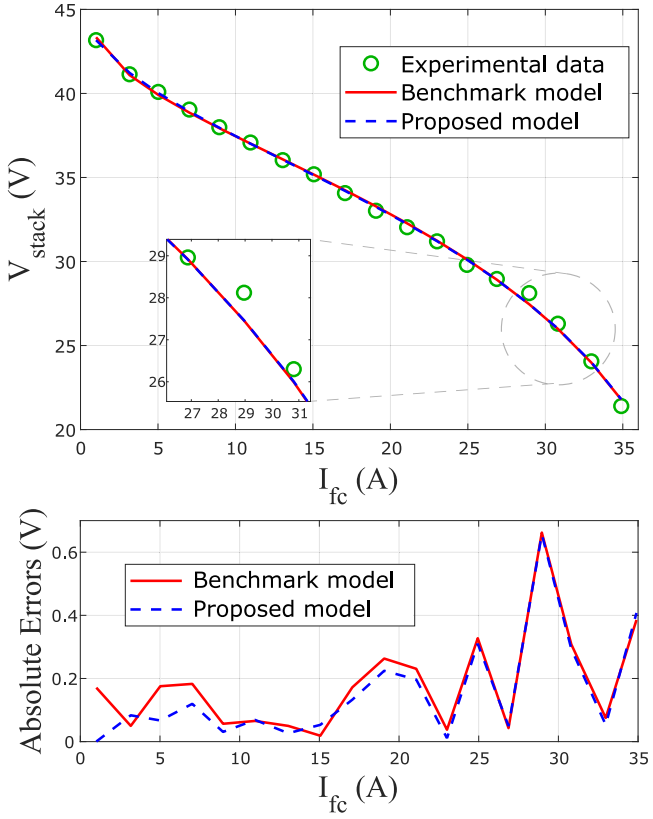

Fig. 6. Best solution for SR-12 500 W PEMFC stack to the two worked models.

55.18 s of the benchmark model.

The statistical results for the optimal point estimated by the algorithm are presented in Table 11. Like the two previous cases, the three first parameters of the benchmark model showed the highest variation, with values of 12.8%, 12.8%, and 35.9%, respectively. Instead, the proposed model presented an RSD lower than 1.38×10^{-7}. In general, the three case studies show that the proposed model has a lower variation across all its parameters.

3.4. The fourth case study

The fourth case study in this research pertains to a newly acquired experimental dataset conducted within the laboratory at the Hydrogen Research Institute of Université du Québec à Trois-Rivières. An open cathode Horizon PEMFC of 500 W serves as the main component of this

Table 10
Results for the SR-12 500 W PEMFC stack.

Benchmark model		Proposed model	
Best solution			
ξ_1	-0.9928	α	0.3007
ξ_2	2.84×10^{-3}	I_0	3.64×10^{-3}
ξ_3	4.38×10^{-5}	R_{eq}	1.00×10^{-4}
ξ_4	-9.54×10^{-5}	β_{eq}	0.1792
λ	24	I_{loss}	1.3011
β	1.75×10^{-1}		
R_C	6.83×10^{-4}		
Comparative statistical results of SSE.			
Best	1.0564	**0.9272**	
Worst	1.0564	**0.9272**	
Average	1.0564	**0.9272**	
Std. dev.	$\mathbf{2.8501 \times 10^{-15}}$	4.5096×10^{-14}	

Table 11
Parameters estimated for the SR-12 500 W PEMFC stack.

Parameter estimated	Mean	Standard deviation	Relative standard deviation
Benchmark model			
ξ_1	-0.9848	1.26×10^{-1}	1.28×10^{-1}
ξ_2	3.15×10^{-3}	4.02×10^{-4}	1.28×10^{-1}
$\boldsymbol{\xi_3}$	$\mathbf{6.54 \times 10^{-5}}$	$\mathbf{2.35 \times 10^{-5}}$	$\mathbf{3.59 \times 10^{-1}}$
ξ_4	-9.54×10^{-5}	3.65×10^{-20}	-3.82×10^{-16}
λ	24	8.87×10^{-12}	3.70×10^{-13}
β	0.1754	6.50×10^{-10}	3.71×10^{-9}
R_C	6.83×10^{-4}	3.11×10^{-11}	4.56×10^{-8}
Proposed model			
α	0.3007	4.81×10^{-9}	1.60×10^{-8}
$\mathbf{I_0}$	$\mathbf{3.64 \times 10^{-3}}$	$\mathbf{5.03 \times 10^{-10}}$	$\mathbf{1.38 \times 10^{-7}}$
R_{eq}	1.00×10^{-4}	6.42×10^{-16}	6.42×10^{-12}
β_{eq}	0.1792	4.81×10^{-10}	2.68×10^{-9}
I_{loss}	1.3011	9.52×10^{-8}	7.31×10^{-8}

experimental set-up and the information provided by the manufacturer is presented in Table 4. A detailed explanation of the entire setup is provided in Section 2.5. The voltage responses of the two models, based on the parameter sets with the lowest error, along with the polarization curve obtained from the experimental test bench, are shown in Fig. 7. The voltage responses of the models are so closely matched that zooming in is required to discern any deviations from the experimental data. Furthermore, the absolute error for both models is below 0.1 V.

The POA algorithm is run 30 times to estimate the set of parameters that minimize the error between the models and the experimental data. By performing multiple executions, the goal is to analyze the error's mean and variation, along with the estimated parameter set. Table 12 displays the statistical results for the error between the models and the measured voltage, as well as the sets of parameters that result in the lowest error for each model. Both models show similar values for the SSE and a negligible standard deviation of nine and eleven orders of magnitude for the benchmark and proposed model, respectively. The development of the two models in terms of error does not encounter significant issues; however, the proposed model yields a lower average computation time (41.42 s), compared to the benchmark model, which has an average time of 166.11 s.

To examine the variation in the solution set estimated by the optimization algorithm, the statistical results for the set of parameters of both models are presented in Table 13. Both models in this table have a standard deviation that is eight orders of magnitude lower than the mean for all parameters, suggesting that the variation in the estimated parameters can be considered insignificant. This has resulted in a marked distinction in this specific case study, compared to the three previous case studies, where the benchmark model showed significant variation in the parameters ξ_1, ξ_2, and ξ_3. It is important to mention that the main difference in the analysis of the experimental data for

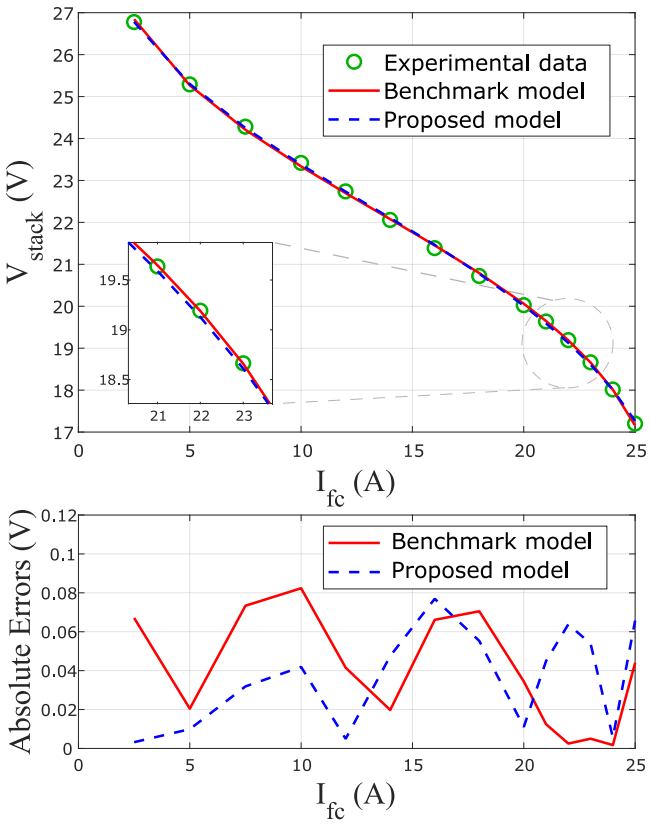

Fig. 7. Best solution for H-500 W PEMFC stack obtained from the two analyzed models considering variable temperature.

Table 12
Results for H-500 W PEMFC stack obtained from the two analyzed models considering variable temperature.

Benchmark model		Proposed model	
Best solution			
ξ_1	-0.8532	α	0.2345
ξ_2	$2.80 \cdot 10^{-3}$	I_0	$5.17 \cdot 10^{-4}$
ξ_3	$9.80 \cdot 10^{-5}$	R_{eq}	$1.00 \cdot 10^{-4}$
ξ_4	$-1.77 \cdot 10^{-4}$	β_{eq}	$3.17 \cdot 10^{-2}$
λ	10	I_{loss}	0.5134
β	$5.03 \cdot 10^{-2}$		
R_C	$8.00 \cdot 10^{-4}$		
Comparative statistical results of SSE.			
Best	$3.1865 \cdot 10^{-2}$	$\mathbf{2.7602 \cdot 10^{-2}}$	
Worst	$3.1865 \cdot 10^{-2}$	$\mathbf{2.7602 \cdot 10^{-2}}$	
Average	$3.1865 \cdot 10^{-2}$	$\mathbf{2.7602 \cdot 10^{-2}}$	
Std. dev.	$1.3821 \cdot 10^{-11}$	$\mathbf{1.1177 \cdot 10^{-13}}$	

the fourth case study is the temperature of the polarization curve. In the first three case studies, the temperature for all the current values is constant. In contrast, the temperature on the experimental test bench demonstrates a proportional rise alongside the current and power increments. The temperature variation is attributed to the PEMFC being an open cathode system, where temperature regulation and cooling are achieved through air convection. Owing to its limited efficiency, this cooling system cannot maintain a constant temperature as power levels increase, unlike closed cathode systems that utilize liquid refrigeration.

4. Conclusions

This work presents a comprehensive review of the semi-empirical models and their application to hybrid prognostic techniques in PEMFCs. It addresses key challenges in parameter identification and their

Table 13
Parameters estimated for the Horizon 500 W fuel cell considering variable temperature.

Parameter estimated	Mean	Standard deviation	Relative standard deviation
Benchmark model			
ξ_1	−0.8532	8.44×10^{-13}	9.89×10^{-13}
ξ_2	$\mathbf{2.80 \times 10^{-3}}$	$\mathbf{7.95 \times 10^{-11}}$	$\mathbf{2.84 \times 10^{-8}}$
ξ_3	9.80×10^{-5}	1.06×10^{-17}	1.08×10^{-13}
ξ_4	-1.77×10^{-4}	2.22×10^{-11}	1.25×10^{-7}
λ	10	1.85×10^{-12}	1.85×10^{-13}
β	5.03×10^{-2}	3.30×10^{-10}	6.56×10^{-9}
R_C	8.00×10^{-4}	6.60×10^{-18}	8.25×10^{-15}
Proposed model			
α	0.2345	1.71×10^{-9}	7.27×10^{-9}
I_0	5.17×10^{-4}	3.92×10^{-11}	7.59×10^{-8}
R_{eq}	1.00×10^{-4}	2.30×10^{-14}	2.30×10^{-10}
β_{eq}	3.17×10^{-2}	1.56×10^{-10}	4.91×10^{-9}
$\mathbf{I_{loss}}$	**0.5134**	$\mathbf{4.29 \times 10^{-8}}$	$\mathbf{8.36 \times 10^{-8}}$

variations, which are important research topics for ensuring the reliability and lifespan of PEMFCs in practical applications.

A comparative study is conducted on two stationary semi-empirical models to evaluate their accuracy and the precision of errors and estimated parameters. This study contrasts a benchmark model, often used in filter-based hybrid prognostic methods, with a proposed semi-empirical model that reduces the benchmark model's seven parameters to five by redefining activation and ohmic losses. Consequently, the boundaries for the optimization algorithm's search region are adjusted. POA, as a new meta-heuristic algorithm, is utilized for parameter estimation, focusing on the accuracy of the SSE. Although minimizing the error between experimental data and the model has been extensively studied, the variability of the estimated parameters has received less attention. Thus, this paper not only evaluates the SSE of both models but also explores the variation and precision of the estimated parameters.

The findings of this comparative study show that both models closely align with the experimental data across four case studies, yielding MAPE values of 0.07%, 0.89%, 0.54%, and 0.18% for the proposed model, and 0.06%, 1.04%, 0.61%, and 0.18% for the benchmark model. Minor discrepancies persist, owing to limitations inherent in semi-empirical models; however, the proposed model exhibits satisfactory accuracy, especially when compared to the benchmark. Moreover, the proposed model demonstrates lower variation in the estimated parameters for the first three case studies, with a maximum RSD of 1.37×10^{-7}.

Additionally, the proposed model's dimensional simplifications reduced the computational load by at least 21.7% across all case studies, offering a balanced trade-off between accuracy and model complexity. This efficiency, combined with the implementation of the POA algorithm, significantly improves the practicality of real-time health monitoring and forecasting for PEMFC systems, particularly in applications such as transportation and energy storage.

Future efforts will apply the proposed model to PHM techniques for PEMFC applications, aiming to streamline real-time health assessments and enhance precision in failure detection and prognostics.

CRediT authorship contribution statement

L.M. Perez: Writing – review & editing, Writing – original draft, Visualization, Software, Methodology, Investigation, Conceptualization. **Samir Jemei:** Writing – review & editing, Supervision, Resources, Methodology, Conceptualization. **Loïc Boulon:** Writing – review & editing, Supervision, Resources, Methodology, Conceptualization. **Alexandre Ravey:** Writing – review & editing, Supervision, Methodology, Conceptualization. **Mohsen Kandidayeni:** Writing – review & editing, Supervision, Resources, Methodology, Conceptualization. **Javier Solano:** Writing – review & editing, Supervision, Resources, Methodology, Conceptualization.

Declaration of competing interest

The authors declare that they have no known competing financial interests or personal relationships that could have appeared to influence the work reported in this paper.

Acknowledgments

This work has been supported by the EIPHI Graduate School (contract ANR-17-EURE-0002) and the Region Bourgogne Franche-Comté.

Data availability

The authors do not have permission to share data.

References

[1] Eyring V, Gillett NP, Rao KMA, Africa RBS, Barreiro M, Bock L, Malinina E, Ruiz L, Sallée J-B, Santer BD, Trewin B, Weigel K, Zhang X, Zhao A, Halenka T, Brazil JAMO, Mitchell D, Gillett N, Rao KA, Barimalala R, Parrillo MB, Bellouin N, Cassou C, Durack P, Kosaka Y, McGregor S, Min S, Morgenstern O, Sun Y, Zhai P, Pirani A, Connors S, Péan C, Berger S, Caud N, Chen Y, Goldfarb L, Gomis M, Huang M, Leitzell K, Lonnoy E, Matthews J, Maycock T, Waterfield T, Yelekçi O, Yu R, Zhou B. Human influence on the climate system. Cambridge, United Kingdom and New York, NY, USA: Cambridge University Press; 2021, http://dx.doi.org/10.1017/9781009157896.005, (Chapter 3).

[2] IEA. Global hydrogen review 2021. Tech. rep., Paris: IEA; 2021, p. 1–221.

[3] Dirkes S, Leidig J, Fisch P, Pischinger S. Prescriptive lifetime management for PEM fuel cell systems in transportation applications, part I: State of the art and conceptual design. Energy Convers Manage 2023;277. http://dx.doi.org/10.1016/j.enconman.2022.116598.

[4] Dirkes S, Leidig J, Fisch P, Pischinger S. Prescriptive lifetime management for PEM fuel cell systems in transportation applications, part II: On-board operando feature extraction, condition assessment and lifetime prediction. Energy Convers Manage 2023;283. http://dx.doi.org/10.1016/j.enconman.2023.116943.

[5] Liu Z, Sun Y, Mao L, Zhang H, Jackson L, Wu Q, Lu S. Efficient fault diagnosis of proton exchange membrane fuel cell using external magnetic field measurement. Energy Convers Manage 2022;266. http://dx.doi.org/10.1016/j.enconman.2022.115809.

[6] Zhang Y, Zhang C, Fan R, Deng C, Wan S, Chaoui H. Energy management strategy for fuel cell vehicles via soft actor-critic-based deep reinforcement learning considering powertrain thermal and durability characteristics. Energy Convers Manage 2023;283:116921. http://dx.doi.org/10.1016/j.enconman.2023.116921.

[7] Wilberforce T, Olabi A, Muhammad I, Alaswad A, Sayed ET, Abo-Khalil AG, Maghrabie HM, Elsaid K, Abdelkareem MA. Recovery of waste heat from proton exchange membrane fuel cells – A review. Int J Hydrog Energy 2024;52:933–72. http://dx.doi.org/10.1016/j.ijhydene.2022.08.069.

[8] Liu G, Qin Y, Wang J, Liu C, Yin Y, Zhao J, Yin Y, Zhang J, Otoo ON. Thermodynamic modeling and analysis of a novel PEMFC-ORC combined power system. Energy Convers Manage 2020;217. http://dx.doi.org/10.1016/j.enconman.2020.112998.

[9] Lu X, Du B, Zhu W, Yang Y, Xie C, Tu Z, Zhao B, Zhang L, Song J, Deng Z. Thermodynamic and dynamic analysis of a hybrid PEMFC-ORC combined heat and power (CHP) system. Energy Convers Manage 2023;292:117408. http://dx.doi.org/10.1016/j.enconman.2023.117408.

[10] Kandidayeni M, Trovão JP, Soleymani M, Boulon L. Towards health-aware energy management strategies in fuel cell hybrid electric vehicles: A review. Int J Hydrog Energy 2022;47:10021–43. http://dx.doi.org/10.1016/j.ijhydene.2022.01.064.

[11] Chen K, Laghrouche S, Djerdir A. Performance analysis of PEM fuel cell in mobile application under real traffic and environmental conditions. Energy Convers Manage 2021;227:113602. http://dx.doi.org/10.1016/j.enconman.2020.113602.

[12] Wang L, Li X, Guo P, Guo S, Yang Z, Pei P. Bibliometric analysis of prognostics and health management (PHM) in hydrogen fuel cell engines. Int J Hydrog Energy 2022;47:34216–43. http://dx.doi.org/10.1016/j.ijhydene.2022.08.024.

[13] Sheng C, Fu J, Li D, Jiang C, Guo Z, Li B, Lei J, Zeng L, Deng Z, Fu X, Li X. Energy management strategy based on health state for a PEMFC/Lithium-ion batteries hybrid power system. Energy Convers Manage 2022;271:116330. http://dx.doi.org/10.1016/j.enconman.2022.116330.

[14] Xiao C, Wang B, Wang C, Yan Y. Design of a novel fully-active PEMFC-lithium battery hybrid power system based on two automatic ON/OFF switches for unmanned aerial vehicle applications. Energy Convers Manage 2023;292. http://dx.doi.org/10.1016/j.enconman.2023.117417.

[15] Yue M, Jemei S, Gouriveau R, Zerhouni N. Review on health-conscious energy management strategies for fuel cell hybrid electric vehicles: Degradation models and strategies. Int J Hydrog Energy 2019;44:6844–61. http://dx.doi.org/10.1016/j.ijhydene.2019.01.190.

[16] Rudolf T, Schurmann T, Schwab S, Hohmann S. Toward holistic energy management strategies for fuel cell hybrid electric vehicles in heavy-duty applications. Proc IEEE 2021;109:1094–114. http://dx.doi.org/10.1109/jproc.2021.3055136.

[17] Hua Z, Zheng Z, Pahon E, Péra M-C, Gao F. A review on lifetime prediction of proton exchange membrane fuel cells system. J Power Sources 2022;529:231256. http://dx.doi.org/10.1016/j.jpowsour.2022.231256.

[18] Sutharssan T, Montalvao D, Chen YK, Wang WC, Pisac C, Elemara H. A review on prognostics and health monitoring of proton exchange membrane fuel cell. Renew Sustain Energy Rev 2017;75:440–50. http://dx.doi.org/10.1016/j.rser.2016.11.009.

[19] Liu H, Chen J, Hissel D, Lu J, Hou M, Shao Z. Prognostics methods and degradation indexes of proton exchange membrane fuel cells: A review. Renew Sustain Energy Rev 2020;123:109721. http://dx.doi.org/10.1016/j.rser.2020.109721.

[20] Alyakhni A, Boulon L, Vinassa J-M, Briat O. A comprehensive review on energy management strategies for electric vehicles considering degradation using aging models. IEEE Access 2021;9:143922–40. http://dx.doi.org/10.1109/ACCESS.2021.3120563.

[21] Ganesh AH, Xu B. A review of reinforcement learning based energy management systems for electrified powertrains: Progress, challenge, and potential solution. Renew Sustain Energy Rev 2022;154:111833. http://dx.doi.org/10.1016/j.rser.2021.111833.

[22] Chen W, Peng J, Ren T, Zhang H, He H, Ma C. Integrated velocity optimization and energy management for FCHEV: An eco-driving approach based on deep reinforcement learning. Energy Convers Manage 2023;296. http://dx.doi.org/10.1016/j.enconman.2023.117685.

[23] Yue M, Jemei S, Zerhouni N, Gouriveau R. Proton exchange membrane fuel cell system prognostics and decision-making: Current status and perspectives. Renew Energy 2021;179:2277–94. http://dx.doi.org/10.1016/j.renene.2021.08.045.

[24] Vichard L, Steiner NY, Zerhouni N, Hissel D. Hybrid fuel cell system degradation modeling methods: A comprehensive review. J Power Sources 2021;506:230071. http://dx.doi.org/10.1016/j.jpowsour.2021.230071.

[25] Jacome A, Hissel D, Heiries V, Gerard M, Rosini S. A review of model-based prognostic for proton exchange membrane fuel cell under automotive load cycling. In: 2019 IEEE vehicle power and propulsion conference. VPPC, 2019, p. 1–5. http://dx.doi.org/10.1109/VPPC46532.2019.8952411.

[26] Kandidayeni M, Macias A, Amamou AA, Boulon L, Kelouwani S, Chaoui H. Overview and benchmark analysis of fuel cell parameters estimation for energy management purposes. J Power Sources 2018;380:92–104. http://dx.doi.org/10.1016/j.jpowsour.2018.01.075.

[27] Liu H, Chen J, Hissel D, Su H. Remaining useful life estimation for proton exchange membrane fuel cells using a hybrid method. Appl Energy 2019;237:910–9. http://dx.doi.org/10.1016/j.apenergy.2019.01.023.

[28] Bressel M, Hilairet M, Hissel D, Bouamama BO. Extended Kalman filter for prognostic of proton exchange membrane fuel cell. Appl Energy 2016;164:220–7. http://dx.doi.org/10.1016/j.apenergy.2015.11.071.

[29] Pei P, Chen D, Wu Z, Ren P. Nonlinear methods for evaluating and online predicting the lifetime of fuel cells. Appl Energy 2019;254. http://dx.doi.org/10.1016/j.apenergy.2019.113730.

[30] Pan R, Yang D, Wang Y, Chen Z. Health degradation assessment of proton exchange membrane fuel cell based on an analytical equivalent circuit model. Energy 2020;207:118185. http://dx.doi.org/10.1016/j.energy.2020.118185.

[31] Aabid SE, Turpin C, Regnier J, Arbigny JD, Horde T, Pessot A. Monitoring of ageing campaigns of PEM fuel cell stacks using a model-based method. Int J Renew Energy Res 2021;11:92–100. http://dx.doi.org/10.20508/ijrer.v11i1.11529.g8114.

[32] Ou M, Zhang R, Shao Z, Li B, Yang D, Ming P, Zhang C. A novel approach based on semi-empirical model for degradation prediction of fuel cells. J Power Sources 2021;488:229435. http://dx.doi.org/10.1016/j.jpowsour.2020.229435.

[33] Julie A, Nadia YS, Simon M, Noureddine Z, der Linden Fabian V, Daniel H. Fuel cell prognosis using particle filter: application to the automotive sector. In: 2022 IEEE 31st international symposium on industrial electronics. ISIE, vol. 2022-June, IEEE; 2022, p. 360–5. http://dx.doi.org/10.1109/ISIE51582.2022.9831770.

[34] Amphlett JC, Baumert RM, Mann RF, Peppley BA, Roberge PR, Harris TJ. Performance modeling of the ballard mark IV solid polymer electrolyte fuel cell I. Mechanistic model development physical properties, assumptions, and approximations. J Electrochem Soc 1995;142.

[35] Ren X, Zhang X, Teng T, Li C. Research on estimation method of fuel cell health state based on lumped parameter model. Energies 2020;13:6425. http://dx.doi.org/10.3390/en13236425.

[36] Kandidayeni M, Soleymani M, Macias A, Trovão JP, Boulon L. Online power and efficiency estimation of a fuel cell system for adaptive energy management designs. Energy Convers Manage 2022;255:115324. http://dx.doi.org/10.1016/j.enconman.2022.115324.

[37] Guo X, Zeng D, Li W, Dong Z, Yu X. Marginalized particle filtering for online parameter estimation of PEMFC applied to hydrogen UAVs. Sustain Energy Technol Assessments 2023;57. http://dx.doi.org/10.1016/j.seta.2023.103265.

[38] Ma R, Xie R, Xu L, Huangfu Y, Li Y. A hybrid prognostic method for PEMFC with aging parameter prediction. IEEE Trans Transp Electrif 2021;7:2318–31. http://dx.doi.org/10.1109/TTE.2021.3075531.

[39] Ettihir K, Boulon L, Becherif M, Agbossou K, Ramadan HS. Online identification of semi-empirical model parameters for PEMFCs. Int J Hydrog Energy 2014;39:21165–76. http://dx.doi.org/10.1016/j.ijhydene.2014.10.045.

[40] Amamou A, Kandidayeni M, Macias A, Boulon L, Kelouwani S. Efficient model selection for real-time adaptive cold start strategy of a fuel cell system on vehicular applications. Int J Hydrog Energy 2020;45:19664–75. http://dx.doi.org/10.1016/j.ijhydene.2020.04.253.

[41] Kandidayeni M, Macias A, Khalatbarisoltani A, Boulon L, Kelouwani S. Benchmark of proton exchange membrane fuel cell parameters extraction with metaheuristic optimization algorithms. Energy 2019;183:912–25. http://dx.doi.org/10.1016/j.energy.2019.06.152.

[42] Hachana O, El-Fergany AA. Efficient PEM fuel cells parameters identification using hybrid artificial bee colony differential evolution optimizer. Energy 2022;250. http://dx.doi.org/10.1016/j.energy.2022.123830.

[43] Alsaidan I, Shaheen MA, Hasanien HM, Alaraj M, Alnafisah AS. A PEMFC model optimization using the enhanced bald eagle algorithm. Ain Shams Eng J 2022;13. http://dx.doi.org/10.1016/j.asej.2022.101749.

[44] Priya K, Rajasekar N. Application of flower pollination algorithm for enhanced proton exchange membrane fuel cell modelling. Int J Hydrog Energy 2019;44:18438–49. http://dx.doi.org/10.1016/j.ijhydene.2019.05.022.

[45] Menesy AS, Sultan HM, Hassan MH, Elsayed SK, Kamel S. Calculating optimal parameters of proton exchange membrane fuel cell. In: 2021 IEEE CHILEAN conference on electrical, electronics engineering, information and communication technologies. CHILECON, IEEE; 2021, p. 1–9. http://dx.doi.org/10.1109/CHILECON54041.2021.9702937.

[46] Sultan HM, Menesy AS, Kamel S, Hasanien HM, Al-Durra A. Identifying optimal parameters of proton exchange membrane fuel cell using water cycle algorithm. IEEE; 2020, p. 176–81. http://dx.doi.org/10.1109/SPIES48661.2020.9242973.

[47] Rao Y, Shao Z, Ahangarnejad AH, Gholamalizadeh E, Sobhani B. Shark smell optimizer applied to identify the optimal parameters of the proton exchange membrane fuel cell model. Energy Convers Manage 2019;182:1–8. http://dx.doi.org/10.1016/j.enconman.2018.12.057.

[48] Ali M, El-Hameed MA, Farahat MA. Effective parameters' identification for polymer electrolyte membrane fuel cell models using grey wolf optimizer. Renew Energy 2017;111:455–62. http://dx.doi.org/10.1016/j.renene.2017.04.036.

[49] Menesy AS, Sultan HM, Korashy A, Kamel S, Jurado F. A modified farmland fertility optimizer for parameters estimation of fuel cell models. Neural Comput Appl 2021;33:12169–90. http://dx.doi.org/10.1007/s00521-021-05821-1.

[50] Sultan HM, Menesy AS, Kamel S, Tostado-Veliz M, Jurado F. Parameter identification of proton exchange membrane fuel cell stacks using bonobo optimizer. In: 2020 IEEE international conference on environment and electrical engineering and 2020 IEEE industrial and commercial power systems Europe. EEEIC / I&CPS Europe, IEEE; 2020, p. 1–7. http://dx.doi.org/10.1109/EEEIC/ICPSEurope49358.2020.9160597.

[51] Yousri D, Mirjalili S, Machado JA, Thanikanti SB, elbaksawi O, Fathy A. Efficient fractional-order modified harris hawks optimizer for proton exchange membrane fuel cell modeling. Eng Appl Artif Intell 2021;100. http://dx.doi.org/10.1016/j.engappai.2021.104193.

[52] Diab AAZ, Tolba MA, El-Magd AGA, Zaky MM, El-Rifaie AM. Fuel cell parameters estimation via marine predators and political optimizers. IEEE Access 2020;8:166998–7018. http://dx.doi.org/10.1109/ACCESS.2020.3021754.

[53] El-Fergany AA, Hasanien HM, Agwa AM. Semi-empirical PEM fuel cells model using whale optimization algorithm. Energy Convers Manage 2019;201. http://dx.doi.org/10.1016/j.enconman.2019.112197, Q1.

[54] El-Fergany AA. Electrical characterisation of proton exchange membrane fuel cells stack using grasshopper optimizer. IET Renew Power Gener 2018;12:9–17. http://dx.doi.org/10.1049/iet-rpg.2017.0232.

[55] Qais MH, Hasanien HM, Turky RA, Alghuwainem S, Loo KH, Elgendy M. Optimal PEM fuel cell model using a novel circle search algorithm. Electron (Switzerland) 2022;11. http://dx.doi.org/10.3390/electronics11121808, Q2.

[56] Rezk H, Olabi A, Ferahtia S, Sayed ET. Accurate parameter estimation methodology applied to model proton exchange membrane fuel cell. Energy 2022;255:124454. http://dx.doi.org/10.1016/j.energy.2022.124454.

[57] Abdel-Basset M, Mohamed R, Abouhawwash M. On the facile and accurate determination of the highly accurate recent methods to optimize the parameters of different fuel cells: Simulations and analysis. Energy 2023;272. http://dx.doi.org/10.1016/j.energy.2023.127083.

[58] Blanco-Cocom L, Botello-Rionda S, Ordoñez LC, Valdez SI. A self-validating method via the unification of multiple models for consistent parameter identification in PEM fuel cells. Energies 2022;15. http://dx.doi.org/10.3390/en15030885.

[59] Losantos R, Montiel M, Mustata R, Zorrilla F, Valiño L. Parameter characterization of HTPEMFC using numerical simulation and genetic algorithms. Int J Hydrog Energy 2022;47:4814–26. http://dx.doi.org/10.1016/j.ijhydene.2021.11.084.

[60] Jacome A, Hissel D, Heiries V, Gerard M, Rosini S. Prognostic methods for proton exchange membrane fuel cell under automotive load cycling: A review. IET Electr Syst Transp 2020;10:369–75. http://dx.doi.org/10.1049/iet-est.2020.0045.

[61] Yue M, Li Z, Roche R, Jemei S, Zerhouni N. Degradation identification and prognostics of proton exchange membrane fuel cell under dynamic load. Control Eng Pract 2022;118:104959. http://dx.doi.org/10.1016/j.conengprac.2021.104959.
[62] Mo ZJ, Zhu XJ, Wei LY, Cao GY. Parameter optimization for a PEMFC model with a hybrid genetic algorithm. Int J Energy Res 2006;30:585–97. http://dx.doi.org/10.1002/er.1170.
[63] Sharaf OZ, Orhan MF. An overview of fuel cell technology: Fundamentals and applications. Renew Sustain Energy Rev 2014;32:810–53. http://dx.doi.org/10.1016/j.rser.2014.01.012.
[64] Trojovský P, Dehghani M. Pelican optimization algorithm: A novel nature-inspired algorithm for engineering applications. Sensors 2022;22. http://dx.doi.org/10.3390/s22030855.
[65] Tuerxun W, Xu C, Haderbieke M, Guo L, Cheng Z. A wind turbine fault classification model using broad learning system optimized by improved pelican optimization algorithm. Machines 2022;10:407. http://dx.doi.org/10.3390/machines10050407.
[66] Mohammed GP, Alasmari N, Alsolai H, Alotaibi SS, Alotaibi N, Mohsen H. Autonomous short-term traffic flow prediction using pelican optimization with hybrid deep belief network in smart cities. Appl Sci 2022;12:10828. http://dx.doi.org/10.3390/app122110828.
[67] Chen Y, Yang B, Guo Z, Wang J, Zhu M, Li Z, Yu T. Dynamic reconfiguration for TEG systems under heterogeneous temperature distribution via adaptive coordinated seeker. Prot Control Mod Power Syst 2022;7:38. http://dx.doi.org/10.1186/s41601-022-00259-6.
[68] Xing S, Zhao C, Zou J, Zaman S, Yu Y, Gong H, Wang Y, Chen M, Wang M, Lin M, Wang H. Recent advances in heat and water management of forced-convection open-cathode proton exchange membrane fuel cells. Renew Sustain Energy Rev 2022;165:112558. http://dx.doi.org/10.1016/j.rser.2022.112558.
[69] Faramarzi A, Heidarinejad M, Mirjalili S, Gandomi AH. Marine predators algorithm: A nature-inspired metaheuristic. Expert Syst Appl 2020;152:113377. http://dx.doi.org/10.1016/j.eswa.2020.113377.
[70] Saremi S, Mirjalili S, Lewis A. Grasshopper optimisation algorithm: Theory and application. Adv Eng Softw 2017;105:30–47. http://dx.doi.org/10.1016/j.advengsoft.2017.01.004.
[71] Yang X-S. Flower pollination algorithms. Elsevier; 2014, p. 155–73. http://dx.doi.org/10.1016/B978-0-12-416743-8.00011-7.